



ELSEVIER

Contents lists available at ScienceDirect

Applied Surface Science

journal homepage: www.elsevier.com/locate/apsusc

Full length article

One-step fabrication of bi- and quad-directional femtosecond laser-induced periodic surface structures on metal with a depolarizer

Taek Yong Hwang^{a,*}, Heedeuk Shin^b, Jeongjin Kang^a, Byounghwak Lee^c, Chunlei Guo^{d,e}

^a Molds & Dies R&D Group, Korea Institute of Industrial Technology, Bucheon 14441, South Korea

^b Department of Physics, Pohang University of Science and Technology, Pohang 37673, South Korea

^c Department of Physics and Chemistry, Korea Military Academy, Seoul 01805, South Korea

^d The Institute of Optics, University of Rochester, New York 14627, USA

^e The Guo China-US Photonics Laboratory, Changchun Institute of Optics, Fine Mechanics, and Physics, Changchun, China

ARTICLE INFO

Keywords:

Femtosecond phenomena
Femtosecond laser processing
Nanostructure fabrication
Laser-induced periodic surface structures

ABSTRACT

With femtosecond (fs) laser pulse irradiation, a simple but efficient technique to fabricate bi- and quad-directional low spatial frequency laser-induced periodic surface structures (BD- and QD-LSFLs) is suggested on metals. By inserting a quartz wedge achromatic depolarizer prior to the focusing optics, we change the polarization of fs laser pulses periodically in one dimension within the laser spot, and find that this method leads to the creation of BD- and QD-LSFLs by simply raster scanning fs laser pulses on Ni. It is also demonstrated that the interval of orientation change of BD-LSFLs can be manipulated with defocus.

1. Introduction

In the past few decades, femtosecond (fs) laser-induced periodic surface structures (LIPSSs) on metals have been paid attention to the field of laser-matter interaction due to their unique capability of controlling the optical, physical, and mechanical properties of metal surfaces with simple and environmentally beneficial fabrication processes [1–7]. Among various types of fs LIPSSs, low spatial frequency LIPSSs (LSFLs) are particularly useful to manipulate the structural color of metal surface by means of diffraction, because the period of LSFLs generated at normal incidence with commonly used Ti:sapphire and Yb-doped fiber fs laser systems falls into the range of visible and near-infrared wavelengths [4,8–10]. Moreover, the range of LSFL period can be easily expanded continuously from near-UV to near-IR wavelengths with the incident beam angle [9,11,12], and the efficiency of a specific order of diffraction can be potentially controlled by creating LSFLs with the blazed grooves [13].

Since the formation of LSFLs is attributable to the interference between the incident p-polarized laser pulses and surface plasmon-polaritons (SPPs), excited by the incident pulses, the orientation (grating vector) of LSFLs only appears within a small angular range close to the polarization direction of fs laser pulses [9,11,14–16]. Due to this restriction, the structural color desired from LSFLs can be sharply observed within a very narrow viewing angle near the angle of diffraction [4,17]. The most common ways of expanding the viewing angle of

structural color are to fabricate LSFLs with multiple orientations by changing the linear polarization direction of a laser beam using a half-wave plate [8,17] and by tailoring the polarization of fs laser within the beam spot so that diffraction occurs efficiently to multiple directions. Recently, by using a spatial light modulator (SLM), full control of laser polarization within laser beam spot is now possible [18], and there also have been a few attempts to utilize this ability to surface nanostructuring [19,20]. However, unfortunately, SLM can be only used at relatively low laser fluence due to low damage threshold and heat accumulation. Currently, without using an SLM, optical vortex beams with radially and azimuthally polarizations and their modified forms have been typically used for LSFL fabrication in most cases [21,22]. Although creating LSFLs with multiple orientations, these types of polarizations have rotational symmetry, and therefore are not well-fitted with raster scanning for seamless production with high productivity.

In this work, under fs laser pulse irradiation, we suggest a highly effective technique to fabricate bi- and quad-directional LSFLs (BD- and QD-LSFLs) on metals by spatially changing the polarization of fs laser beam with a quartz wedge achromatic depolarizer (QWAD). We also demonstrate that the changing interval of BD-LSFL orientation can be adjusted by slightly defocusing the fs laser pulses from the surface of metal.

* Corresponding author.

E-mail address: taekyong@kitech.re.kr (T.Y. Hwang).

<https://doi.org/10.1016/j.apsusc.2019.07.025>

Received 17 May 2019; Received in revised form 1 July 2019; Accepted 3 July 2019

Available online 04 July 2019

0169-4332/ © 2019 Elsevier B.V. All rights reserved.

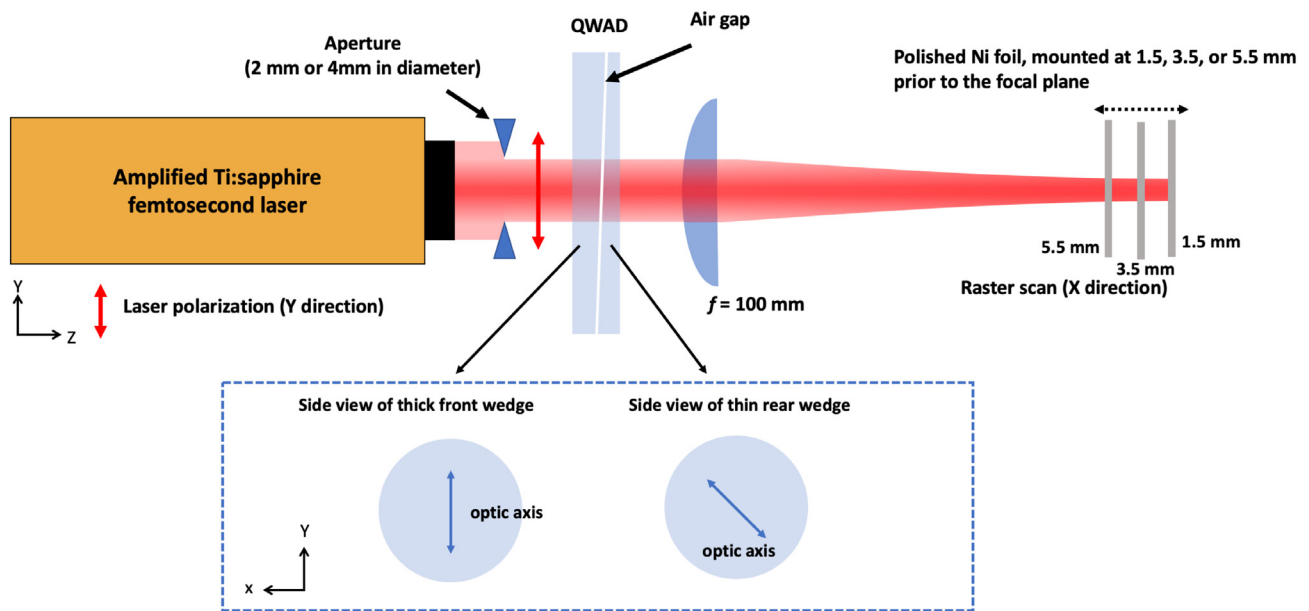


Fig. 1. Schematic of BD- and QD-LSFL fabrication in our experiments. Polished Ni samples are raster scanned in the x direction. Optic axes of front and rear wedges of QWAD follow the coordinate described in the dashed box.

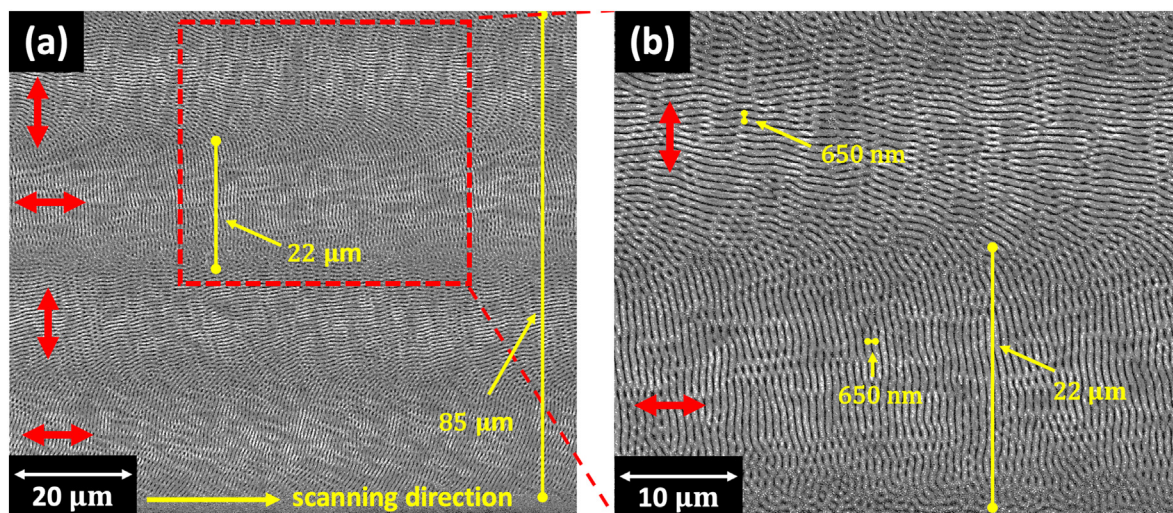


Fig. 2. SEM images of BD-LSFLs fabricated with a defocus of 1.5 mm. Two orientations of BD-LSFLs are fabricated twice within a single scan line. Spatial interval of orientation change in BD-LSFL across the scan line is about 22 μm .

2. Methods and materials

An amplified Ti:sapphire fs laser system that generates 120-fs at a central wavelength of 800 nm used in our experiments, and operates with an average power of 5 W at a 1 kHz repetition rate. A $1/e^2$ intensity diameter of fs laser output is about 10 mm, and apertures with a diameter of 2 mm and 4 mm are used, in case we need to reduce the size of laser beam output, as shown in Fig. 1. To fabricate LSFLs on Ni, Ni foils with a thickness of 2 mm are mechanically polished with 80-nm-grade colloidal silica, and the average roughness of polished Ni surfaces is measured to be 9.4 nm.

Before fs laser pulses hit the lens, the polarization of linearly polarized laser beam is tailored one-dimensionally by using a QWAD. As described in Fig. 1, QWAD is consist of two crystal quartz wedges with a wedge angle of 2° assembled with 0.2 mm air gap between two wedges. The front and rear wedge thicknesses at the center are 4.8 mm and 2.4 mm, respectively, and the angle between the optic axes of two wedges is 45° . In our experiments, fs laser pulses always hit the front

wedge at normal incidence, and their polarization is parallel to the crystal axis of the front wedge and is 45° rotated from the crystal axis of the rear wedge. For the incident fs pulses, the front wedge of QWAD only changes their incident angle to about 3.1° at the front surface of the rear wedge. With the off-normal incidence at the front surface of the rear wedge, the mismatch between the polarization direction of incident fs laser pulses and the optic axis of the rear wedge leads to the separation of fs pulses into two with a very small angular deviation of propagation due to the birefringence of quartz, whose refractive indices for the electric field components of fs laser pulses parallel and perpendicular to the optic axis of quartz are 1.547 and 1.5383 at our laser wavelength of 800 nm, respectively [23]. Following Snell's law [24], the angular deviation of propagation between two fs pulses separated can be calculated as 0.018° . The two separated fs pulses each have polarizations parallel and perpendicular to the optic axis of the rear wedge.

After QWAD, fs laser pulses are slightly focused onto the sample surface with a 100 mm focal length plano-convex lens, while the sample

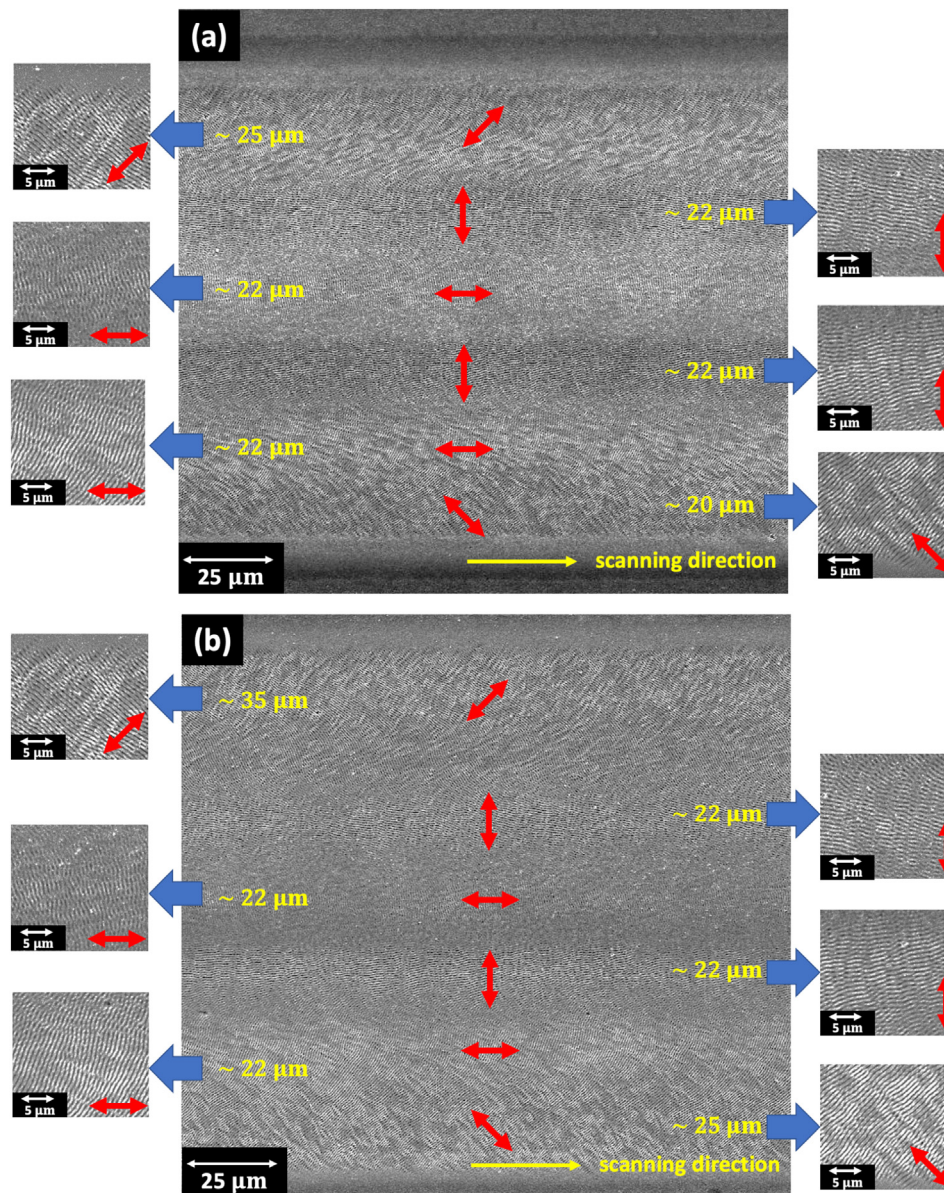


Fig. 3. SEM images of QD-LSFLs produced by a single raster scan with laser fluences of (a) 0.17 J/cm² and (b) 0.34 J/cm². The amount of defocus used here is 1.5 mm. Lengths described in the SEM images show the thicknesses of each orientation of LSFLs within QD-LSFLs. Thicknesses of two additional orientations at the edges of the scan line increase with laser fluence.

is always raster-scanned with a velocity of 1 mm/s in all our experiments. The sample is mounted at 1.5 mm, 3.5 mm, or 5.5 mm prior to the focal plane for the fabrication of BD- and QD-LSFLs. The semi-minor (semi-major) axes of $1/e^2$ intensity at these positions are measured about 75 μm (105 μm), 180 μm (210 μm), and 270 μm (295 μm), respectively, where the elliptical beam shape is originated from the separation of fs laser pulses by QWAD. The laser fluence is calculated by taking into account the elliptical shape of beam. The ablation of polished Ni samples starts to occur at a laser fluence of 0.016 J/cm².

The surface textures of BD- and QD-LSFLs are measured by using a scanning electron microscope (SEM). Lengths written in Figs. 3–5 denote the thicknesses of each orientation of LSFLs within BD- or QD-LSFLs, and double-headed (red) and single-headed (yellow) arrows in all SEM images indicate the orientation of LSFLs and the direction of the raster scan, respectively, where the orientation of LSFLs is defined as the grating vector of LSFLs. All SEM images show BD- or QD-LSFLs within a single raster scan line.

3. Results and discussion

We start by irradiating fs laser pulses to polished Ni surfaces with a fluence of 0.11 J/cm² at normal incidence after the polarization of fs laser pulses is manipulated with a QWAD. A polished Ni sample is mounted about 1.5 mm prior to the focal planes. Under these experimental conditions, we generate bi-directional LSFLs (BD-LSFLs), where LSFLs are clearly oriented with two distinct perpendicular directions, as shown in Fig. 2(a). The thickness of each scan line with BD-LSFLs is about 85 μm, and the orientation of BD-LSFLs rotates 90° every 22 μm. Consequently, the two perpendicular orientations of LSFLs in BD-LSFLs are formed twice within the scan line. Regardless of their orientations, the period of LSFLs is in the range of 650 ± 30 nm, as shown in Fig. 2(b).

Next, laser fluence increases to 0.17 J/cm², while other conditions are kept the same. The thickness of fs laser scan line widens to 130 μm due to higher laser fluence. Different from the low fluence case shown in Fig. 2, two additional orientations of LSFLs with 45° rotated from the

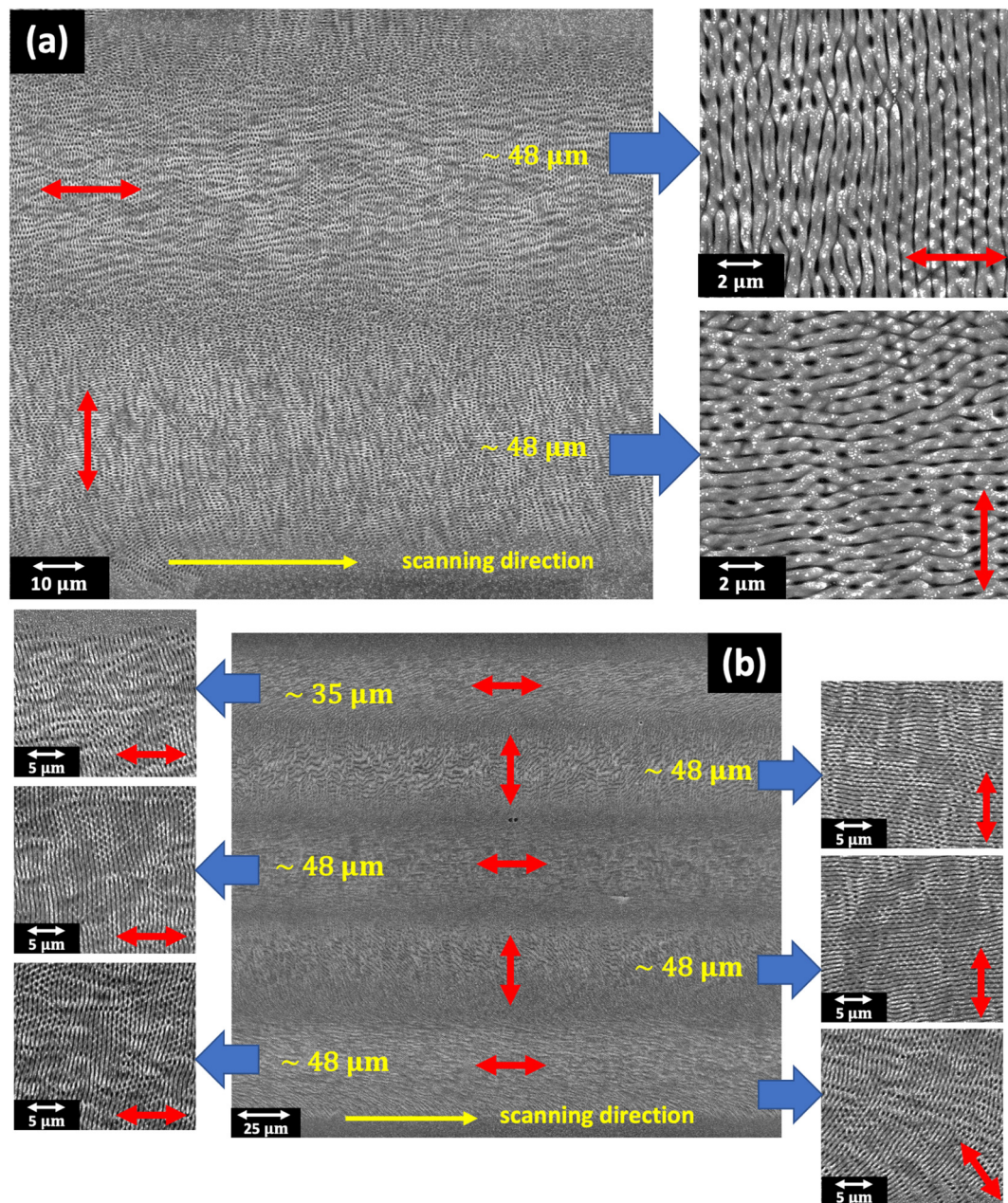


Fig. 4. SEM images of BD-LSFLs produced at 3.5 mm defocus with laser fluences of (a) 0.07 J/cm^2 and (b) 0.13 J/cm^2 .

orientations of BD-LSFLs come into view at the two edges of each scan line, and eventually contribute to the formation of quad-directional LSFLs (QD-LSFLs), as clearly viewed in Fig. 3(a). When we further elevate the laser fluence to 0.34 J/cm^2 , the area of LSFLs with these newly added orientations expands to the edges of the scan line as the thickness of the scan line increases, as described in Fig. 3(b); however, in terms of the period of BD-LSFL groove and the interval of BD-LSFL orientation change in the center of the scan line, no apparent differences are observed from BD-LSFLs in Figs. 2 and 3.

Fig. 4 shows BD-LSFLs produced on Ni positioned at 3.5 mm prior to the focal plane. Compared to the previous cases shown in Figs. 2 and 3, the fs laser processed line becomes thicker at the surface of Ni due to an additional defocus of 2 mm. With a laser fluence of 0.07 J/cm^2 , the two orthogonal orientations of BD-LSFLs are clearly formed only once within the raster scan line and are observed twice at a laser fluence of 0.13 J/cm^2 , as shown in Fig. 4(b). However, two additional orientations consisting of QD-LSFLs at the edges described earlier are rarely

observed with the edges of the scan line at a defocus of 3.5 mm. Compared Fig. 3 to Fig. 4(b), the orientation of BD-LSFLs at the top edge of the scan line in Fig. 4(b) is in the horizontal direction, different from that in Fig. 3.

From Figs. 3 and 4, it is easily noticed that the interval of orientation change of BD-LSFLs significantly increases from $22 \mu\text{m}$ to $48 \mu\text{m}$ with defocus. This increase in the spatial interval of orientation change of BD-LSFLs also holds with a longer defocus of 5.5 mm, and the interval becomes about $75 \mu\text{m}$ as clearly visualized in Fig. 5. Our observation indicates that the interval of the orientation change can be readily controlled with defocus.

Our understanding of LSFLs formation on metal is largely based on the interference between the incident fs laser pulses and SPPs excited by the incident laser pulses [9,14]. According to this mechanism, the orientation (grating vector) of LSFLs is parallel to the polarization of incident laser pulse for linear polarization [9,14] and the major axis of ellipse for elliptical polarization [25] at normal incidence. Therefore, it

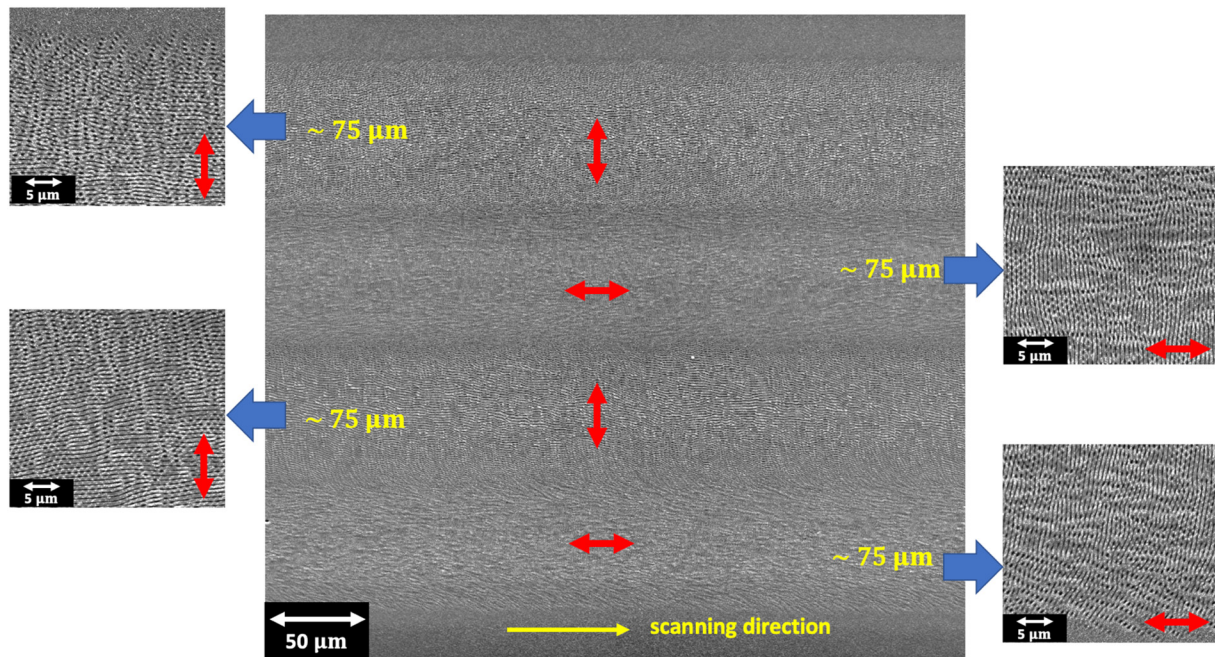


Fig. 5. SEM images of BD-LSFLs on Ni produced at 5.5 mm defocus with a fluence of 0.12 J/cm^2 .

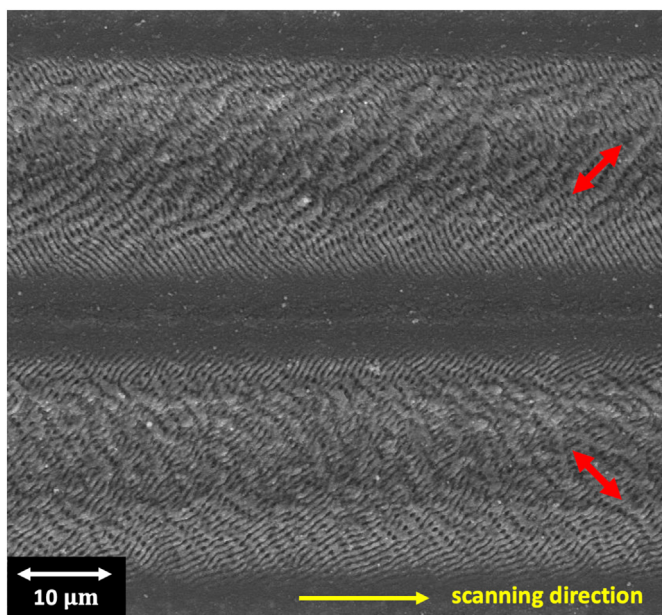


Fig. 6. SEM image of BD-LSFLs produced without defocus. Orientations of LSFLs in two lines produced by a single raster scan are perpendicular to each other, and clearly indicate that the polarizations of fs pulses separated into two by QWAD are orthogonal.

is essential to obtain the polarization direction of fs laser pulses at the sample surface to understand the formation of BD- and QD-LSFLs.

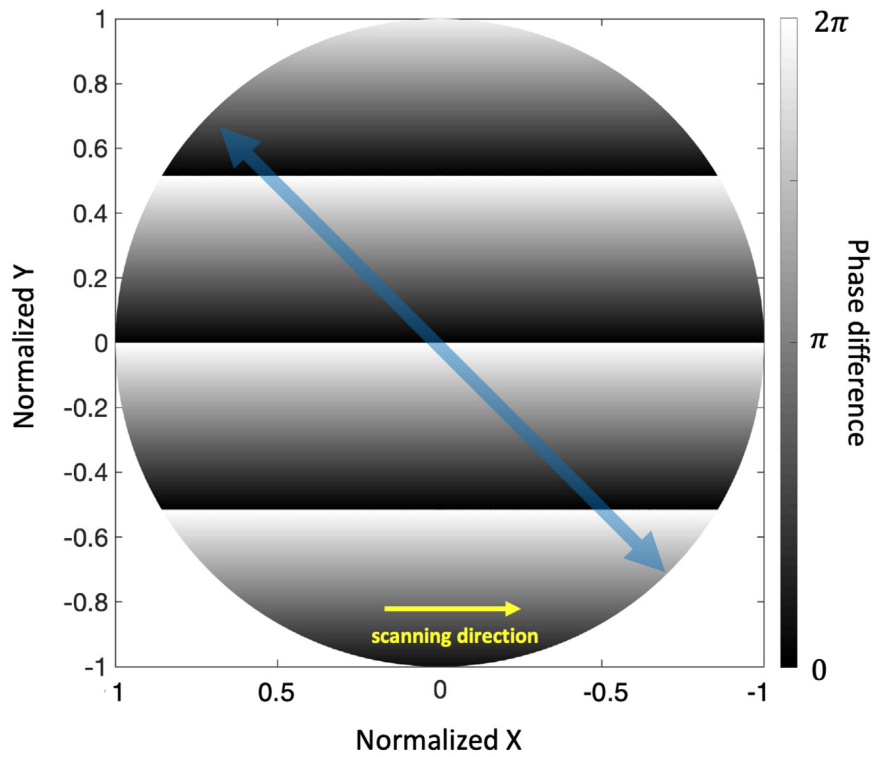
Before evaluating the polarization of fs laser pulses in detail, we first consider the effect of QWAD on fs pulses. QWAD separates fs pulses into the two orthogonally polarized fs pulses with a small angular deviation of 0.018° . The angular deviation and polarizations of the two separated pulses both are confirmed by our observation that the fs laser pulses are completely separated about $31 \mu\text{m}$ without defocusing and their polarizations are orthogonal to each other, as shown in Fig. 6. The sizes of fs laser spots mentioned in Section 2 for the three defocused distances are much bigger than their separation, most part of the two orthogonally polarized fs pulses are spatially overlapped, and therefore the

effective polarization within the overlapped region can be determined by the orientations and phase differences of electric fields of two separated fs pulses.

In Fig. 7, the wrapped phase difference between two orthogonally polarized fs pulses right after QWAD and the corresponding polarization for each phase difference are calculated by considering that the angular difference in the propagation of two separated fs pulses is 0.018° [24,26]. Although the polarization direction of fs pulses changes across the laser spot, the orientation of linear polarization and the major axis of elliptical polarization are limited to the horizontal and vertical directions, described in Fig. 7. Due to this limit, LSFLs can have two orientations with QWAD, parallel to either the polarization direction of linear polarization or the major axis of elliptical polarization. Consequently, the formation of BD-LSFLs results from tailored polarization of fs laser pulse led by the superposition of the electric fields of these two separated and orthogonally polarized fs laser pulses with continuously changing phase difference across the scan line.

The formation of QD-LSFLs can be simply understood in a similar manner. In fact, the angular deviation between the separated fs pulses leads to the creation of field intensity unbalance toward the edges of the scan line, where the field from the closer laser spot affects more. Furthermore, while changes in the separation of two fs pulses are insignificantly small with defocused distances used in our experiments, the degree of field intensity unbalance becomes more significant as the size of laser spot gets smaller with a smaller defocus. Therefore, two additional orientations for QD-LSFLs, parallel and perpendicular to the optic axis of the rear wedge, can appear at the two edges of the scan line only with the smallest defocus of 1.5 mm , and are barely observable with larger defocused distances due to negligible field intensity unbalance resulting from much larger spot sizes compared to the spatial distance between two separated fs pulses.

Further evidence can be obtained by reducing the diameter of the fs laser beam with the aperture described in Fig. 1. By using the aperture, the spot size of fs laser pulses can be significantly reduced, and eventually enlarges the area of unbalanced field intensity region at the edges within the scan line even with a larger amount of defocus. As shown in Fig. 8, two orientations of LSFLs parallel and perpendicular to the optic axis of the rear edge are revealed independently at the edges of the scan line, while these are not clearly observed without the aperture



Phase difference	0	$\pi/4$	$\pi/2$	$3\pi/4$	π	$5\pi/4$	$3\pi/2$	$7\pi/4$	2π
Polarization	↔	↻	↻	↻	↕	↻	↻	↻	↔

Fig. 7. Wrapped phase difference between two separated fs pulses right after QWAD. Double headed arrow (blue) denotes the optic axis of the rear wedge, and the polarizations of two separated fs pulses are parallel and perpendicular to the optic axis. Both X and Y axes are normalized by the $1/e^2$ intensity radius of fs laser pulses incident on QWAD.

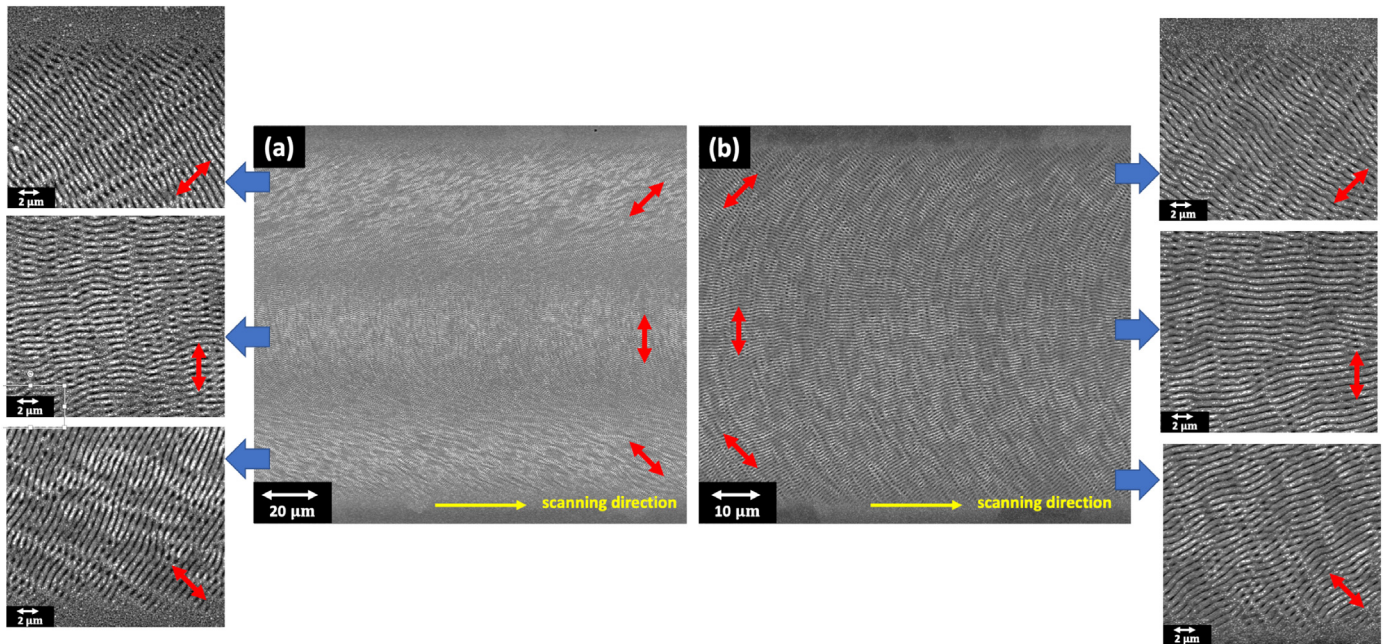


Fig. 8. SEM image of LSFs with three orientations generated by using apertures prior to QWAD with a defocus of 3.5 mm. Diameters of apertures are (a) 4 mm and (b) 2 mm. Except the apertures, other conditions are the same as those for the fabrication of BD-LSFLs in Fig. 4(b).

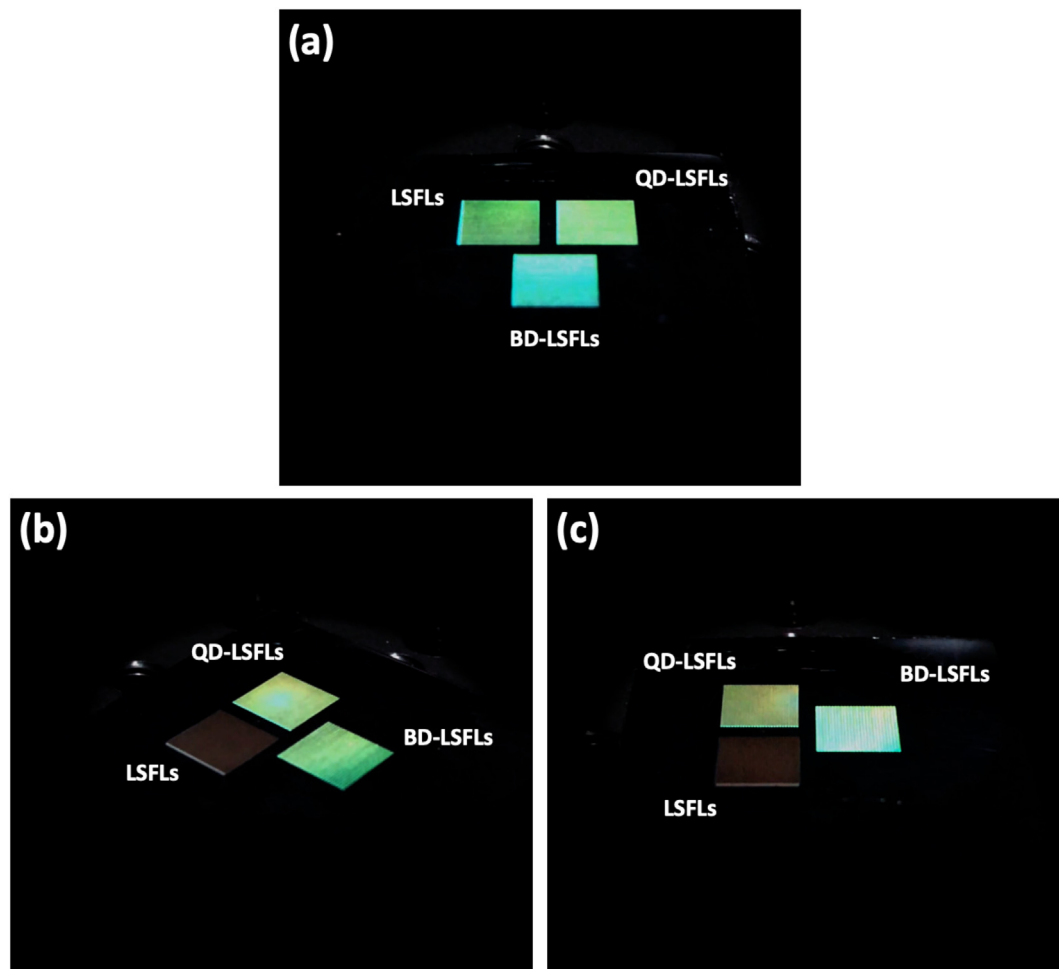


Fig. 9. Diffraction from LSFLs, BD-LSFLs, and QD-LSFLs with rotation angles of (a) 0° , (b) 45° , and (c) 90° . The sample is rotated about the surface normal under white light illumination. The rotation angle is defined as 0° when LSFLs with a single orientation show structural colors.

described early in Fig. 4(b).

It is worth noting how the laser fluence itself can be used to change from QD-LSFLs to BD-LSFLs as shown in Figs. 2 and 3. In Fig. 3, all four orientations consisting of QD-LSFLs can be clearly shown within the scan line; however, as the laser fluence reduces, only the area of two orientations at the edges of scan line shrinks. These orientations are completely gone at the smallest fluence used with a defocus of 1.5 mm and BD-LSFLs eventually form, as shown in Fig. 2.

Lastly, we demonstrate that BD- and QD-LSFLs can be used to change the optical properties of metal surface. In Fig. 9, the sample with LSFLs, BD-LSFLs, and QD-LSFLs is mounted on the rotation stage, and illuminated by white light emitting diodes at an incident angle of 5° . The sample is observed at an angle of 55° , near the -1st order diffraction angle for blue-green color in the visible while rotated about its surface normal. As clearly shown in Fig. 9, different from LSFLs with a single orientation, BD-LSFLs and QD-LSFLs display structural colors with a much broad angular range than LSFLs with a single orientation, and therefore can create the multidirectional colorization of metal surface through diffraction.

4. Conclusion

To conclude, using fs laser pulse irradiation, a concise technique to fabricate BD- and QD-LSFLs is suggested on metal. By inserting a quartz wedge achromatic depolarizer prior to the focusing optics, we control the fs laser polarization periodically within the laser spot, and find that this control leads to the creation of BD- and QD-LSFLs by raster

scanning metal surfaces. We also find that the changing period of BD-LSFL orientation can be controlled by adjusting an amount of defocus during raster scanning. It is also demonstrated that BD- and QD-LSFLs can be potentially useful to control the optical properties of metal surface with multidirectional colorization through diffraction.

Acknowledgments

This work was supported by the Ministry of Planning and Budget, Korea Institute of Industrial Technology. We thank T. K. Lee and H. J. Kim at Korea Institute of Industrial Technology for technical assistance.

References

- [1] A.Y. Vorobyev, C. Guo, Direct femtosecond laser surface nano/microstructuring and its applications, *Laser Photonics Rev.* 7 (2013) 385–407, <https://doi.org/10.1002/lpor.201200017>.
- [2] J. Bonse, S. Höhm, S. Kirner, A. Rosenfeld, J. Krüger, Laser-induced periodic surface structures (LIPSS) - a scientific evergreen, *Conf. Lasers Electro-Optics*, 23 2016, https://doi.org/10.1364/CLEO_SI.2016.STh1Q.3 STh1Q.3.
- [3] J. Bonse, S.V. Kirner, S. Höhm, N. Epperlein, D. Spaltmann, A. Rosenfeld, J. Krüger, Applications of Laser-induced Periodic Surface Structures (LIPSS), (2017), p. 100920N, <https://doi.org/10.1117/12.2250919>.
- [4] A.Y. Vorobyev, C. Guo, Colorizing metals with femtosecond laser pulses colorizing metals with femtosecond laser pulses, *Appl. Phys. Lett.* 041914 (2012) 28–31, <https://doi.org/10.1063/1.2834902>.
- [5] Z. Vassilia, S. Emmanuel, B. Marios, S. Emmanuel, T. Panagiotis, H.A. Spiros, F. Costas, Biomimetic artificial surfaces quantitatively reproduce the water repellency of a lotus leaf, *Adv. Mater.* 20 (2008) 4049–4054, <https://doi.org/10.1002/adma.200800651>.
- [6] H. Gau, S. Herminghaus, P. Lenz, R. Lipowsky, Liquid morphologies on structured

- surfaces: from microchannels to microchips, *Science* (80-) 283 (1999) 46, <https://doi.org/10.1126/science.283.5398.46>.
- [7] R. Buividas, M. Mikutis, S. Juodkakis, Surface and bulk structuring of materials by ripples with long and short laser pulses: recent advances, *Prog. Quantum Electron.* 38 (2014) 119–156, <https://doi.org/10.1016/j.pquantelec.2014.03.002>.
- [8] B. Dusser, Z. Sagan, H. Soder, N. Faure, J.P. Colombier, M. Jourlin, E. Audouard, Controlled nanostructures formation by ultra fast laser pulses for color marking, *Opt. Express* 18 (2010) 2913–2924, <https://doi.org/10.1364/OE.18.002913>.
- [9] T.Y. Hwang, C. Guo, Angular effects of nanostructure-covered femtosecond laser induced periodic surface structures on metals, *J. Appl. Phys.* 108 (2010) 73523, , <https://doi.org/10.1063/1.3487934>.
- [10] A.A. Ionin, S.I. Kudryashov, S.V. Makarov, L.V. Seleznev, D.V. Sinitsyn, E.V. Golosov, O.A. Golosova, Y.R. Kolobov, A.E. Ligachev, Femtosecond laser color marking of metal and semiconductor surfaces, *Appl. Phys. A Mater. Sci. Process.* 107 (2012) 301–305, <https://doi.org/10.1007/s00339-012-6849-y>.
- [11] H.U. Lim, J. Kang, C. Guo, T.Y. Hwang, Manipulation of multiple periodic surface structures on metals induced by femtosecond lasers, *Appl. Surf. Sci.* 454 (2018) 327–333, <https://doi.org/10.1016/j.apsusc.2018.05.158>.
- [12] C.A. Zuhlke, G.D. Tsibidis, T. Anderson, E. Stratakis, G. Gogos, D.R. Alexander, Investigation of femtosecond laser induced ripple formation on copper for varying incident angle, *AIP Adv.* 8 (2018) 15212, , <https://doi.org/10.1063/1.5020029>.
- [13] T.Y. Hwang, C. Guo, Femtosecond laser-induced blazed periodic grooves on metals, *Opt. Lett.* 36 (2011) 2575, <https://doi.org/10.1364/OL.36.002575>.
- [14] J.E. Sipe, J.F. Young, J.S. Preston, H.M. van Driel, Laser-induced periodic surface structure. I. Theory, *Phys. Rev. B* 27 (1983) 1141, <https://doi.org/10.1103/PhysRevB.27.1141>.
- [15] A.Y. Vorobyev, V.S. Makin, C. Guo, Periodic ordering of random surface nanostructures induced by femtosecond laser pulses on metals, *J. Appl. Phys.* 101 (2007) 34903, , <https://doi.org/10.1063/1.2432288>.
- [16] A.M. Bonch-Bruевич, M.N. Libenson, V.S. Makin, V.V. Trubaev, Surface electromagnetic waves in optics, *Opt. Eng.* 31 (1992) 718, <https://doi.org/10.1117/12.56133>.
- [17] T. Jwad, P. Penchev, V. Nasrollahi, S. Dimov, Laser induced ripples' gratings with angular periodicity for fabrication of diffraction holograms, *Appl. Surf. Sci.* 453 (2018) 449–456, <https://doi.org/10.1016/j.apsusc.2018.04.277>.
- [18] I. Moreno, J.A. Davis, T.M. Hernandez, D.M. Cottrell, D. Sand, Complete polarization control of light from a liquid crystal spatial light modulator, *Opt. Express* 20 (2012) 364–376, <https://doi.org/10.1364/OE.20.000364>.
- [19] B. Lam, J. Zhang, C. Guo, Generation of continuously rotating polarization by combining cross-polarizations and its application in surface structuring, *Opt. Lett.* 42 (2017) 2870–2873, <https://doi.org/10.1364/OL.42.002870>.
- [20] O.J. Allegre, W. Perrie, S.P. Edwardson, G. Dearden, K.G. Watkins, Laser micro-processing of steel with radially and azimuthally polarized femtosecond vortex pulses, *J. Opt.* 14 (2012) 85601, , <https://doi.org/10.1088/2040-8978/14/8/085601>.
- [21] M. Beresna, M. Gecevičius, P.G. Kazansky, T. Gertus, Radially polarized optical vortex converter created by femtosecond laser nanostructuring of glass, *Appl. Phys. Lett.* 98 (2011) 201101, , <https://doi.org/10.1063/1.3590716>.
- [22] J. JJ Nivas, E. Allahyari, F. Cardano, A. Rubano, R. Fittipaldi, A. Vecchione, D. Paparo, L. Marrucci, R. Bruzzese, S. Amoroso, Surface structures with unconventional patterns and shapes generated by femtosecond structured light fields, *Sci. Rep.* 8 (2018) 13613, , <https://doi.org/10.1038/s41598-018-31768-w>.
- [23] G. Ghosh, Dispersion-equation coefficients for the refractive index and birefringence of calcite and quartz crystals, *Opt. Commun.* 163 (1999) 95–102, [https://doi.org/10.1016/S0030-4018\(99\)00091-7](https://doi.org/10.1016/S0030-4018(99)00091-7).
- [24] E. Hecht, *Optics*, 4th ed., Addison-Wesley, Reading, Massachusetts, 2002.
- [25] Y. Tang, J. Yang, B. Zhao, M. Wang, X. Zhu, Control of periodic ripples growth on metals by femtosecond laser ellipticity, *Opt. Express* 20 (2012) 25826–25833, <https://doi.org/10.1364/OE.20.025826>.
- [26] T. Todorov, L. Nikolova, N. Tomova, Polarization holography. 2: polarization holographic gratings in photoanisotropic materials with and without intrinsic birefringence, *Appl. Opt.* 23 (1984) 4588–4591, <https://doi.org/10.1364/AO.23.004588>.